

Transfer Print Integration of Waveguide-Coupled Germanium Photodiodes Onto Passive Silicon Photonic ICs

Nan Ye, *Student Member, IEEE*, Grigorij Muliuk^{1b}, *Student Member, IEEE*, Jing Zhang, *Student Member, IEEE*, Amin Abbasi, *Student Member, IEEE*, Antonio Jose Trindade, Chris Bower, Dries Van Thourhout^{1b}, *Senior Member, IEEE*, and Gunther Roelkens^{1b}, *Senior Member, IEEE*

(Post-Deadline Paper)

Abstract—We demonstrate the integration of waveguide-coupled germanium photodiodes onto passive silicon waveguide circuits by means of transfer printing. This involves the release of the photodiodes from the silicon-on-insulator source wafer by undercutting the buried oxide layer while protecting the back-end stack. Tethers were formed to keep the released photodiode coupons in place. Coupons were then transfer printed to a silicon photonic target wafer with an alignment accuracy better than $\pm 1 \mu\text{m}$. 0.66 A/W waveguide-referred photodiode responsivity at 1550 nm was obtained. High-speed measurements yielded open eye diagrams at 40 Gb/s.

Index Terms—Photodiodes, transfer printing.

I. INTRODUCTION

MICRO-TRANSFER printing (μTP or transfer printing), proposed by Rogers *et al.* [1] is a novel integration technology in which materials or devices can be selectively removed from their source wafer and transferred to a new substrate in a massively parallel way, making use of a structured elastomeric polydimethylsiloxane (PDMS) stamp. One of the biggest merits of this technology is that dense arrays of different devices realized on their source wafer can be selectively picked and printed on the target substrate, with high yield and high alignment accuracy ($< \pm 1.5 \mu\text{m}$; 3σ [2]), potentially scaling out the device array to e.g., a 200 mm passive silicon photonic wafer, containing silicon or silicon nitride waveguide circuits, as schematically

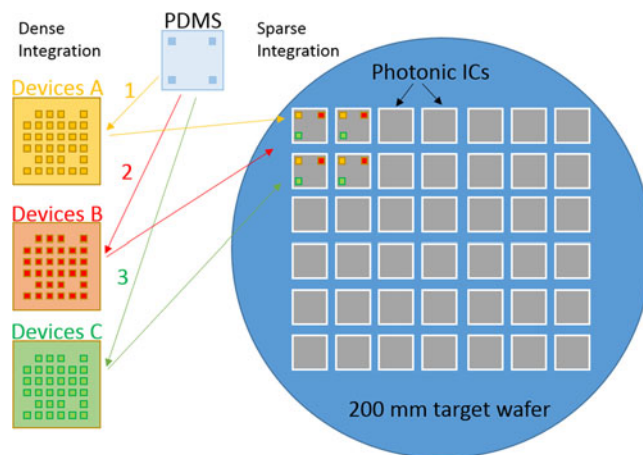


Fig. 1. Schematic demonstration of area magnification in transfer printing. Densely patterned devices A (yellow), B (red) and C (green) on the source can be picked and printed—massively parallel—on a target wafer in a sparse way using a patterned PDMS stamp.

illustrated in Fig. 1. Using this technique, one can build a complete photonic integrated circuit in a cost- and time-effective manner by transfer printing various active devices on a passive integrated circuit and interconnect these devices using a wafer-scale passivation and metallization.

Transfer-printing technology is particularly interesting for the scalable integration of III-V semiconductors on silicon photonic integrated circuits and some results have already been reported in [3]–[5]. On the other hand, silicon-germanium (SiGe) active devices (including high-speed photodiodes [6] and electro-absorption modulators [7]) can be monolithically integrated on a silicon-on-insulator platform, but typically the full process flow comprises more than 30 mask levels to be processed in a complementary metal oxide semiconductor (CMOS) fab, resulting in a fairly long turnaround time and high cost, especially for applications where the density of active devices required in the photonic integrated circuit is small. This significantly hampers the development of photonic integrated circuits on this platform.

Manuscript received October 27, 2017; accepted November 21, 2017. Date of publication November 23, 2017; date of current version March 1, 2018. This work was supported by the European Union's Horizon 2020 Research and Innovation Programme under Grant Agreement 645314 (TOP-HIT). (Nan Ye and Grigorij Muliuk contributed equally to this work.) (Corresponding author: Grigorij Muliuk.)

N. Ye, G. Muliuk, A. Abbasi, J. Zhang, D. Van Thourhout, and G. Roelkens are with the Photonics Research Group, Department of Information Technology, Center of Nano- and Biophotonics, Ghent University–IMEC, Ghent B-9052, Belgium (e-mail: Nan.ye@ugent.be; Grigorij.muliuk@ugent.be; Amin.Abbasi@ugent.be; Jingzhan.Zhang@ugent.be; Dries.vanhourhout@ugent.be; Gunther.roelkens@ugent.be).

A. J. Trindade is with the X-Celeprint Ltd., Cork T12R5CD, Ireland (e-mail: Ajosetrindade@x-celeprint.com).

C. Bower is with the X-Celeprint Ltd., Triangle Park 27709, NC, USA (e-mail: Cbower@x-celeprint.com).

Color versions of one or more of the figures in this paper are available online at <http://ieeexplore.ieee.org>.

Digital Object Identifier 10.1109/JLT.2017.2777509

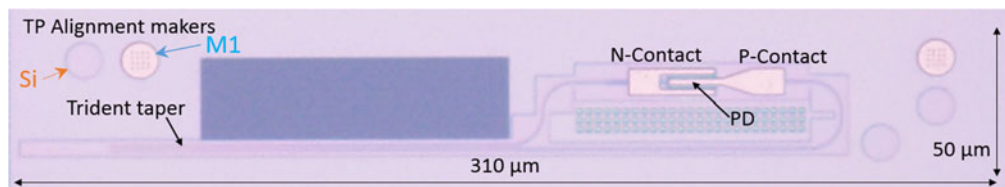


Fig. 2. Microscope image of the germanium photodiode coupon.

Using a transfer-printing approach one can print SiGe devices realized on a source wafer in a dense array onto a silicon photonic target wafer. This way, a new photonic integrated circuit generation requires only refabricating the passive silicon photonics wafer, hence allowing for a significantly improved turnaround time. Moreover, the integration of SiGe photonic devices with e.g., silicon nitride waveguide circuits [8] is enabled where monolithic integration cannot be easily achieved.

This paper is the extension of an ECOC post-deadline publication [9] and presents the transfer printing of germanium photodiodes (Ge PDs) on a passive silicon-on-insulator (SOI) target waveguide circuit, including both the process development and the device characterization. In Section II we discuss the design of the transfer printing compatible device coupons, together with the alignment tolerant waveguide coupling structure. The release and transfer printing process is discussed in Section III where the most important technological challenges together with the final process flow are presented. Transfer printing with an alignment accuracy better than ± 1 micrometer is demonstrated. The post-processing steps are discussed as well. Section IV describes the measurement results. We report a waveguide-referred responsivity of 0.66 A/W at 1550 nm wavelength, together with 40 Gbit/s operation of the photodetector.

II. COUPON DESIGN

The p-i-n Ge PDs were fabricated in imec's fully integrated Si Photonics Platform (iSIPP25G [10]) along with Si modulators and various passive devices. The wafers go through a process flow described in [11]. Fig. 2 depicts the microscope image of the Ge PD coupon. The light is fed into the germanium photodiode (PD) using a trident taper structure similar to the structure described in other works [12]. By not combining the two waveguides of the trident on the silicon coupon but rather feeding these waveguides to opposite sides of the Ge PD, good lateral misalignment tolerance can be obtained. This is illustrated in Fig. 3 showing the simulated coupling loss as a function of lateral misalignment, indicating a negligible impact of a lateral misalignment of ± 1 μm , for a 130 μm long taper structure. The coupon size is 310 \times 50 μm . No large contact pads are defined in this coupon design, which allows a denser packing of the coupons on the source wafer, as well as an easier release of the coupons. In order to enable high alignment accuracy transfer printing, alignment marker circles were integrated, which aid the automatic alignment (discussed later). High marker contrast is of paramount importance, hence, two different types of markers were used to evaluate their performance: markers etched 150 nm in the silicon device layer and M1 markers (Fig. 2).

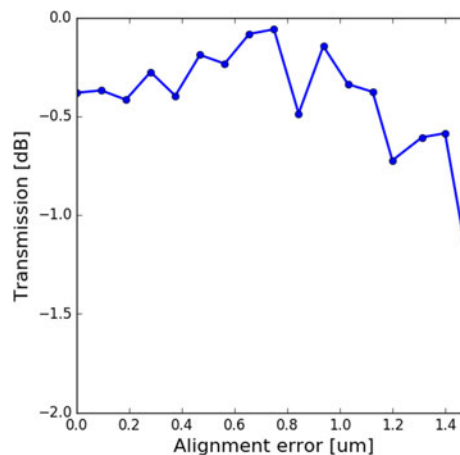


Fig. 3. Impact of the lateral misalignment on the coupling efficiency of the trident taper structure.

III. RELEASE, TRANSFER PRINTING AND POST PROCESSING

A. Stress Process

Fig. 4 depicts the process flow for the Ge PD release and transfer printing. On a standard iSIPP25G chip (Fig. 4(a)) we deposit a 75 nm thick silicon nitride layer protection layer to protect the back-end stack during further processing steps (Fig. 4(b)). In a first lithography step we form 310 \times 50 μm coupon mesas by dry-etching the back-end stack down to the silicon device layer using $\text{CF}_4:\text{SF}_6:\text{H}_2$. Because of the thick back-end stack and dry-etching non-uniformity, we end the process by immersing the structures in a buffered hydrofluoric etch (BHF) for 30 seconds to remove all residual SiO_2 in the trenches (Fig. 4(c)). Next, a 1 micrometer plasma-enhanced chemical vapor deposition (PECVD) amorphous silicon (A-Si) protection layer is deposited at 180 $^\circ\text{C}$ (Fig. 4(d)), which will protect the back-end stack of the coupons during the buried oxide underetch. As the bottom side of the coupon consists of a uniform silicon device layer, the device will also be protected from that side during the release etch. With a second lithography and dry etch ($\text{CF}_4:\text{SF}_6:\text{H}_2$) we locally expose the buried oxide and form the tether structures (Fig. 4(e)).

The design of the tether structures is shown in Fig. 5. The tether design was optimized as to hold the coupon in place after the release, while allowing to be easily broken during device pick-up, avoiding damage of or debris on the device coupons. Triangular tether structures were found to work most efficiently. However, the width of the narrowest points has to be carefully controlled: the optimal width is about 1.2–1.5 micrometer. When the tether width is below 1 μm , the tethers are too weak to hold the coupons suspended and these collapse on the sili-

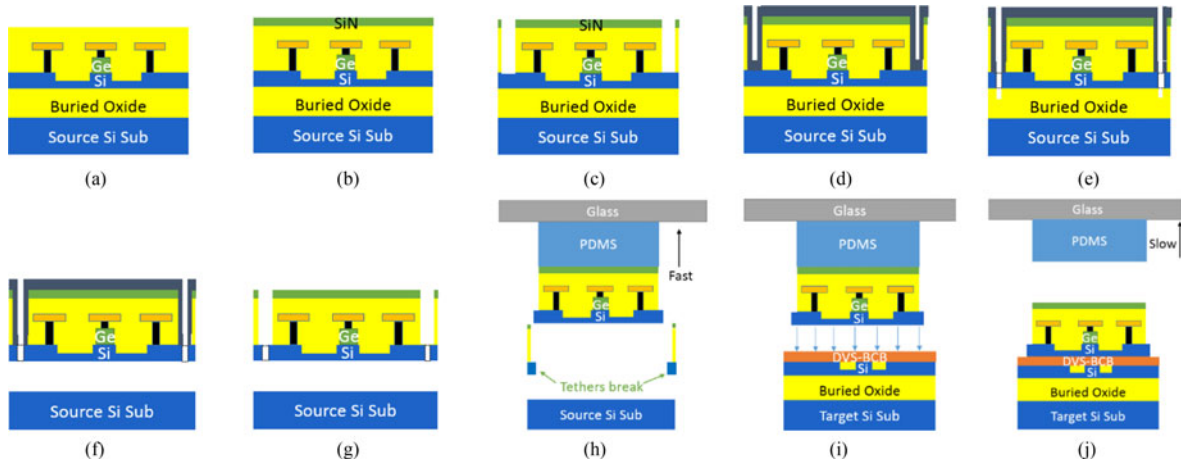


Fig. 4. Coupon release and transfer printing process.

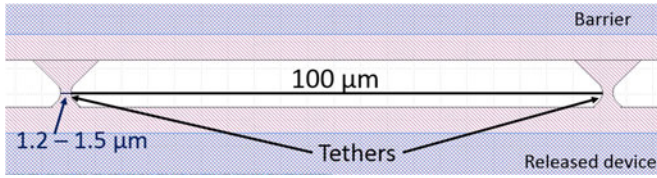


Fig. 5. Schematic image of photodiode tether structures.

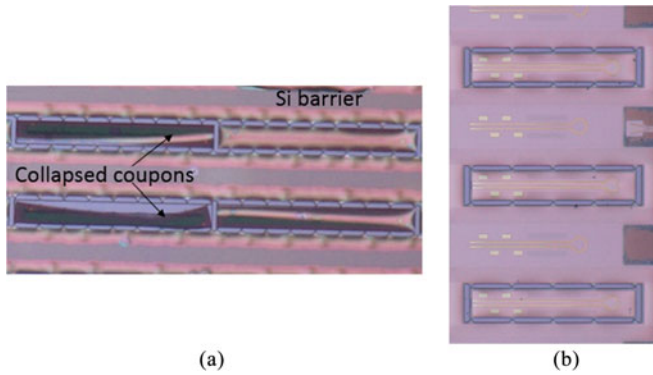


Fig. 6. (a) Released silicon devices with poor stress compensation showing that coupons bend and collapse. (b) Released silicon devices with good stress compensation.

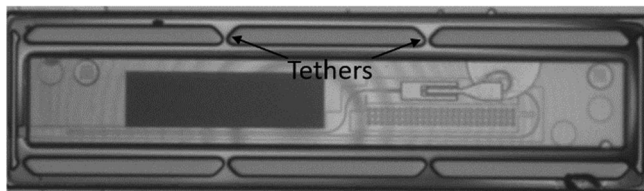


Fig. 7. Microscope image of a released germanium photodiode coupon.

con substrate. Whereas when the tether width exceeds $2 \mu\text{m}$, the coupon attachment to the surroundings is too strong and it becomes difficult to pick the coupons using the PDMS stamp. Immersing the structures into a 40% HF solution for around 13 minutes allows underetching the buried oxide layer (Fig. 4(f)), while the coupons are kept in place using the tethers.

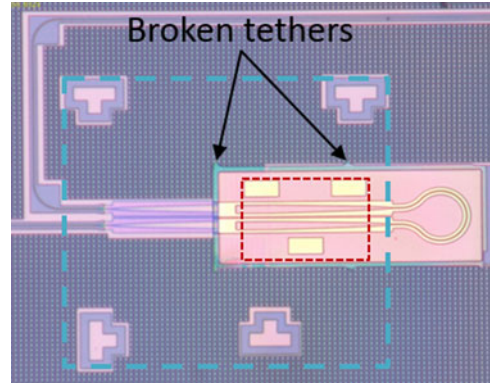


Fig. 8. Transfer printed silicon device with a passive waveguide coupling structure. Transfer printing alignment markers on the target (blue) and on the source (red) are shown. The broken tethers that held the coupons in place on the source wafer can be identified as well.

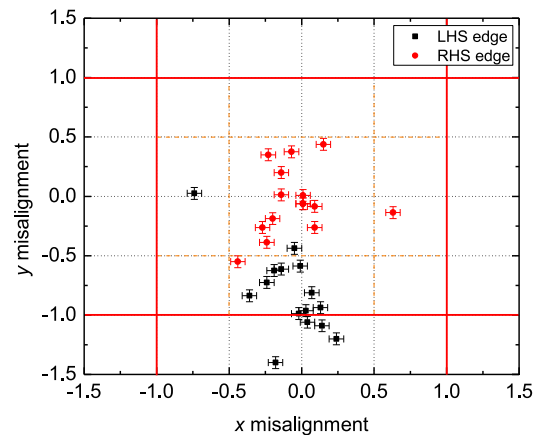


Fig. 9. Misalignment measurement for printed coupons measured at the left and right-hand side of the coupon.

Finally, by dry etching using $\text{CF}_4:\text{SF}_6:\text{H}_2$ one can uniformly remove the A-Si layer in the final process step (Fig. 4(g)), resulting in transfer-printing-ready coupons.

Stress management of the device layer stack of the released coupons is essential. Residual stress in the layer stack causes

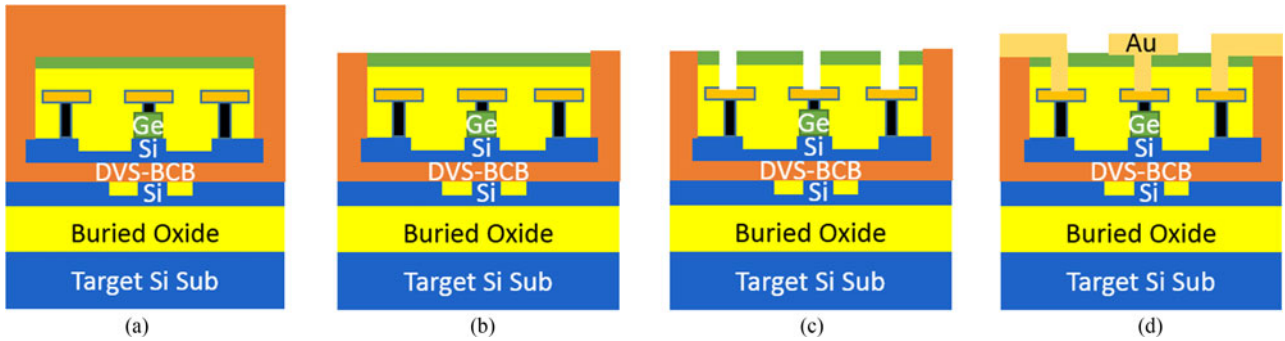


Fig. 10. Post processing schematics of printed coupon.

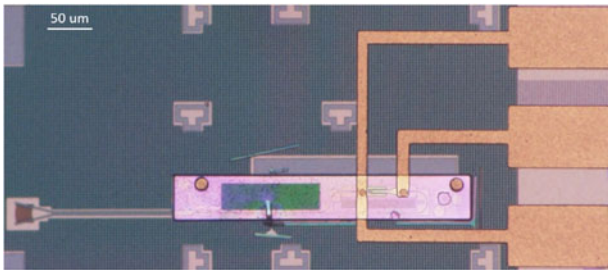


Fig. 11. Microscope image of a germanium photodiode coupon printed on the target wafer with the Au contact pads deposited.

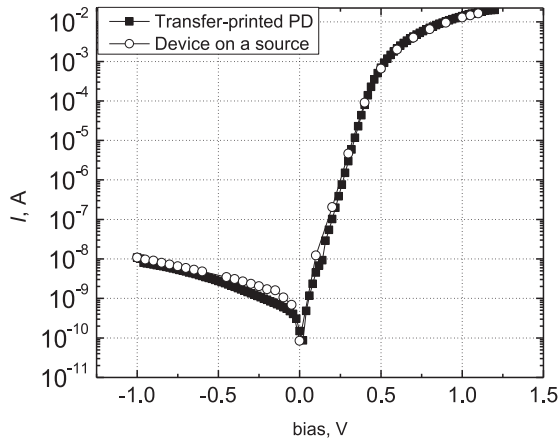


Fig. 12. Measured I-V characteristics of the transfer printed germanium photodiode, compared with the I-V of a similar device on the source wafer.

released coupons to bend and collapse on the substrate. Potentially it can also introduce micro-cracks in the thin silicon device layer allowing the HF to penetrate the device coupon during the release etch. The comparison of released coupons without and with proper stress management (by optimizing the deposition conditions of the back-end layers) is shown in Fig. 6, after the removal of the amorphous silicon encapsulation.

The top view image of a released germanium photodiode coupon is demonstrated in Fig. 7. Here the silicon coupon is now a thin membrane, held in place by triangular tether structures to the surrounding area.

B. Transfer Printing Process

The transfer-printing was carried out using an X-Celeprint micro-TP100 lab-scale printer. By laminating a structured elas-

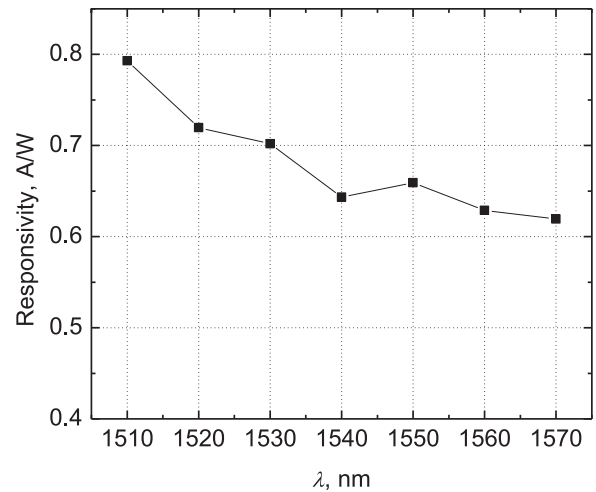


Fig. 13. Waveguide-referred responsivity of the transfer printed germanium photodiode as a function of wavelength.

tomeric PDMS stamp to the suspended germanium photodiode coupon and quickly moving it in the vertical direction, one is able to break the silicon tethers in their weakest (narrowest) points and hence pick up the released coupon (Fig. 4(h)). Printing is performed by laminating the picked coupon on the stamp against a divinylsiloxane-bis-benzocyclobutene (DVS-BCB, soft-cured at 180 °C) coated SOI target substrate (Fig. 4(i)). By slowly moving the stamp in the vertical direction the Ge PD coupon remains attached to the SOI target wafer (Fig. 4(j)). We demonstrate the high-alignment accuracy (better than $\pm 1 \mu\text{m}$) by transfer printing individual coupons with passive waveguide couplers printed on an SOI target (Fig. 8). Alignment is performed using COGNEX image recognition software [13] and for this purpose markers were designed on the source coupon (150 nm etch Si - marked in red in Fig. 8) and the target wafer (marked in blue in Fig. 8). One can train the software for auto-alignment by selecting these markers, locating their geometric centers and the difference between them (so-called off-center auto alignment method). By picking the coupon and bringing it in close proximity to the target wafer, the software can recognize both sets of markers and allow automatic alignment of the coupon with respect to target with high precision.

We assessed the alignment further by printing 15 similar silicon device coupons to a silicon photonic target wafer, auto-aligned by the COGNEX software. Using scanning electron

microscopy (SEM) we were able to assess the alignment in both x- and y-directions. The results are presented in Fig. 9. The red points on the graph depict misalignment measured on the left-hand side of coupons and black points depict misalignment on the right-hand side.

As one can see, most of the measured left-hand side points are within the ± 500 nm misalignment window in x- and in y-direction. The right-hand side measurement results however, show significantly higher misalignment values in particularly in y. This is an indication of a rotational misalignment, a problem that needs to be tackled by a better angular alignment of the source and target wafer in the transfer printing tool. For our purpose, however, the light couples to and from the device coupon from only one side and therefore the results are sufficient to transfer print.

C. Post-Processing

The device post-processing – after printing of the photodetector coupons - is schematically depicted in Fig. 10. We start by spin-coating a thick (~ 3 micron) DVS-BCB layer on the target substrate and fully curing it at 280°C (Fig. 10(a)). The purpose is to planarize the device to allow for the metallization of the coupon. The DVS-BCB is then etched back using $\text{SF}_6:\text{O}_2$ plasma (Fig. 10(b)). With a first lithography and dry etch ($\text{CF}_4:\text{SF}_6:\text{H}_2$) the Cu contacts are opened (Fig. 10(c)). In a second lithography step we define $1.2\ \mu\text{m}$ thick Au metal tracks using lift-off. Important to note is that after the window opening, Cu contacts tend to oxidize very quickly, therefore before depositing the Au metal pads, the devices were immersed in an acetic acid: H_2O (1:9) solution for about 10 minutes to remove the thin oxide layer on top of the Cu metal contacts. Fig. 11 depicts the final germanium photodiode coupon transfer printed on the silicon target circuit, consisting of a single mode waveguide connected to a grating coupler. High alignment accuracy printing achieved using the high contrast metal markers on the source coupon.

IV. MEASUREMENT RESULTS

A. Static Characteristics

I-V curve of the measured device is depicted in Fig. 12. Here the black points represent the I-V of the transfer printed device and it is compared to a similar device on the source where the same post-processing schematics were applied, as discussed in Section III. One can see a very good match of these two curves with the dark current measured to be $12\ \text{nA}$ at $-1\ \text{V}$ biasing and a series resistance of $29.6\ \Omega$.

The waveguide-referred device responsivity curve versus wavelength is shown in Fig. 13. A responsivity of $0.66\ \text{A/W}$ at $1550\ \text{nm}$ is demonstrated. These p-i-n iSIPP25G photodetectors were specified with a device responsivity of $0.8\ \text{A/W}$ at $1550\ \text{nm}$, which is higher than the value for the transfer printed device coupon because of the trident taper coupling losses.

B. Dynamic Characteristics

Small signal characterization of the Ge PD using an Agilent 67 GHz Network Analyzer was carried out. By biasing the photodiode at $-0.5\ \text{V}$ a slowly rolling-off frequency response

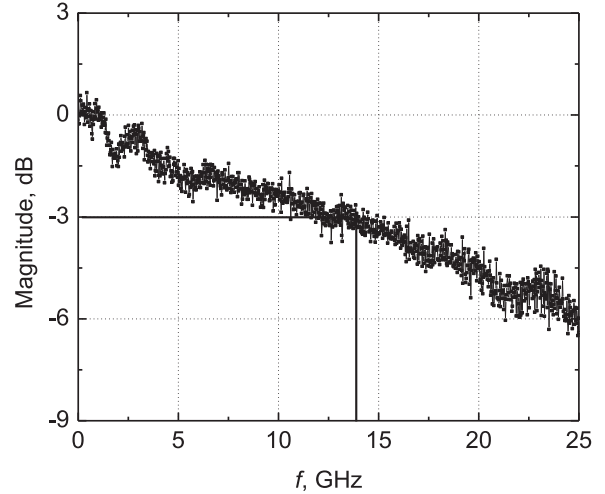


Fig. 14. Small signal measurement result at a wavelength of $1550\ \text{nm}$. The device was biased at $-0.5\ \text{V}$.

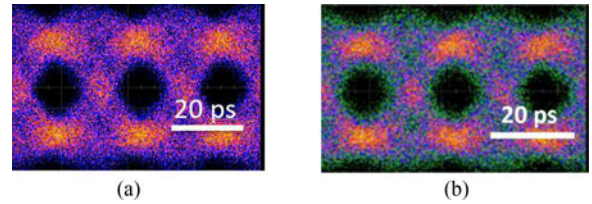


Fig. 15. Eye diagrams for (a) 40 Gbit/s PRBS pattern length 2^7-1 and (b) 40 Gbit/s PRBS pattern length 2^{15} .

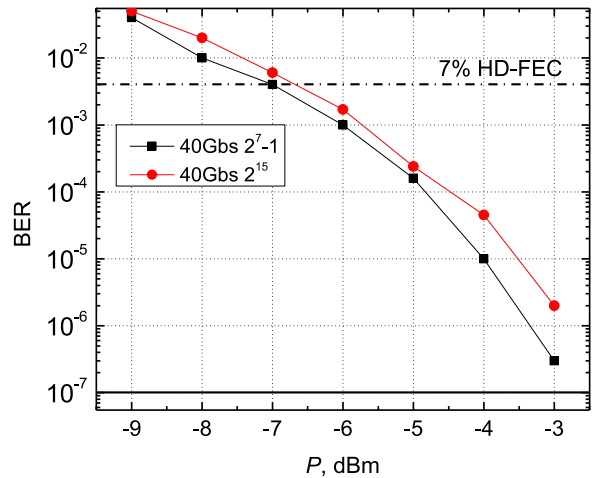


Fig. 16. Bit-error rates as a function of received optical power at 40 Gbit/s.

is obtained with a 3 dB bandwidth at $14\ \text{GHz}$ (Fig. 14). This behavior is attributed to the electrode structure as shown in Fig. 11 not being optimized for high-speed performance.

Large signal measurements were performed using a Keysight M8195A arbitrary waveform generator (AWG) which was driving a $28\ \text{GHz}$ LiNbO_3 modulator. A pseudo random bit sequence (PRBS) with 2^7-1 and 2^{15} pattern lengths at $40\ \text{Gbit/s}$ Non-Return-Zero On Off Keying (NRZ-OOK) were generated to measure the eye diagrams using a Keysight real time oscilloscope. Fig. 15 depicts the eyes at $40\ \text{Gbit/s}$ using pattern lengths of 2^7-1 and 2^{15} . Fig. 16 depicts the bit error rate curve, which for both cases reaches below the 7% HD-FEC limit.

V. CONCLUSION

In this paper we demonstrate the transfer printing of high speed germanium photodiodes on a silicon-on-insulator passive waveguide circuit. We managed to successfully release the device, while leaving the back end stack intact. After picking and printing with high alignment accuracy we demonstrated high efficiency coupling between the target waveguide and the device coupon. We obtained 0.66 A/W responsivity and open eye diagrams at 40 Gbit/s. This demonstration paves the way to apply transfer printing for the realization of complex photonic integrated circuits on a wafer-scale, comprising potentially both Si/Ge photonic and electronic devices as well as III-V optoelectronic components, in a cost-effective way and with a short turnaround time.

REFERENCES

- [1] X. Feng *et al.*, "Competing fracture in kinetically controlled transfer printing," *Langmuir*, vol. 23, pp. 12555–12560, 2007.
- [2] C. A. Bower *et al.*, "Transfer printing: An approach for massively parallel assembly of microscale devices," in *Proc. Electron. Compon. Technol. Conf.*, 2008, pp. 1105–1109.
- [3] A. De Groote *et al.*, "Transfer-printing-based integration of single-mode waveguide-coupled III-V-on-silicon broadband light emitters," *Opt. Express*, vol. 24, no. 13, pp. 13754–13762, 2016.
- [4] J. Zhang *et al.*, "A silicon photonics fiber-to-the-home transceiver array based on transfer-printing-based integration of III-V photodetectors," *Opt. Express*, vol. 25, no. 13, pp. 14290–14299, 2017.
- [5] B. Corbett *et al.*, "Transfer print techniques for heterogeneous integration of photonic components," *Prog. Quantum Electron.*, vol. 52, pp. 1–17, 2017.
- [6] H. Chen *et al.*, "100 Gbps RZ data reception in 67 GHz Si-contacted germanium waveguide p-i-n photodetectors," *J. Lightw. Technol.*, vol. 35, no. 4, pp. 722–726, Feb. 2017.
- [7] Y. Tang *et al.*, "50 Gb/s hybrid silicon traveling-wave electroabsorption modulator," *Opt. Express*, vol. 19, no. 7, pp. 5811–5816, 2011.
- [8] R. Baets *et al.*, "Silicon Photonics: Silicon nitride versus silicon-on-insulator," in *Proc. Opt. Fiber Commun. Conf. Exhib.*, 2016, Paper Th3J.1.
- [9] G. Muliuk *et al.*, "Transfer print integration of 40 Gbps germanium photodiodes onto silicon photonic ICs," in *Proc. Eur. Conf. Opt. Commun.*, 2017, Paper Th.PDP.C.4.
- [10] M. Pantouvaki *et al.*, "Active Components for 50 Gb/s NRZ-OOK optical interconnects in a silicon photonics platform," *J. Lightw. Technol.*, vol. 35, no. 4, pp. 631–638, Feb. 2017.
- [11] P. Verheyen *et al.*, "Highly uniform 25 Gbps Si photonics platform for high-density, low-power WDM optical interconnects," in *Proc. Integr. Photon. Res., Silicon Nanophoton. Conf.*, 2014, Paper IW3A.4.
- [12] K. Itoh, K. Yuki, Y. Hayashi, and J. Suzuki, "Vertical trident coupler for 3D optical interconnection," in *Proc. Group IV Photon.*, 2016, Paper ThC3.
- [13] Cognex Vision Pro Machine Vision, [Online]. Available: <http://www.cognex.com/products/machine-vision/visionpro-vision-software/>. Accessed on: Oct. 2017.

Nan Ye received the B.Sc. degree from the Beijing University of Chemical Technology, Beijing, China, in 2008, the M.Sc. degree from the Institute of Semiconductors, Chinese Academy of Sciences, Beijing, China, in 2011, and the Ph.D. degree from Tyndall National Institute, Cork, Ireland, in 2015. After studying at the Tyndall National Institute, he worked as a Researcher with the Interuniversity Microelectronics Center, Leuven, Belgium, in 2017, focusing on the hybrid integration of Si/Ge and III-V devices on a silicon photonics platform.

Grigorijs Muliuk received the B.Sc. degree in telecommunication engineering from Vilnius University, Vilnius, Lithuania, in 2013, and the European M.Sc. degree in photonics engineering from Ghent University, Ghent, Belgium, Free Brussels University, Brussels, Belgium, and the University of St. Andrews, St. Andrews, U.K. He is currently working toward the Ph.D. degree in photonics at the Photonics Research Group, Department of Information Technology, Ghent University–IMEC, Ghent, Belgium. His research interests include silicon and III-V device integration using transfer printing technology.

Amin Abbasi received the B.Sc. degree in applied physics and the M.Sc. degree in laser physics from the University of Tabriz, Tabriz, Iran, in 2007 and 2009, respectively, and the Ph.D. degree in photonics from Ghent University, Ghent, Belgium in 2016. He was involved with high-speed direct modulation of heterogeneously integrated devices, electroabsorption modulators, and high speed photodiodes. His current research focuses on microwave photonics for communication applications.

Jing Zhang received the B.Sc. degree in physics and M.Sc. degree in optics from Northwest University Xi'an, China, 2009 and 2012, respectively. He is currently working toward the Ph.D. degree in photonics at the Photonics Research Group, Department of Information Technology, Ghent University–IMEC, Ghent, Belgium. His research interests include heterogeneous integration of III-V on Si devices, tunable and narrow linewidth laser, integrated coherent receiver, and transfer printing integration of III-V optoelectronic components.

Antonio Jose Trindade received the M.Sc. degree in physics engineering in 2011 from the University of Aveiro, Aveiro, Portugal, where he worked on organic light emitting devices and organic photovoltaics, and the Ph.D. degree in 2015 from the University of Strathclyde, Glasgow, U.K, where he worked on micro-LEDs and transfer-print technologies. His research interests include heterogeneous integration, micro-transfer-printing, device prototyping, light-emitting semiconductors, and microdisplays.

Chris Bower received the B.S. and Ph.D. degrees in physics from the University of North Carolina at Chapel Hill, Chapel Hill, NC, USA, in 1996 and 2000, respectively. He has more than 15 years of experience in the fabrication and packaging of electronic and photonic devices, both at the nanoscale and the microscale levels. For the past seven years, he led microtransfer printing technology development at Semprius, Inc. His research interests include three-dimensional integration of integrated circuits, heterogeneous integration of compound semiconductors onto nonnative substrates, and the fabrication of low-cost, large-format electronics using novel assembly methods.

Dries Van Thourhout received the Master's degree in physical engineering and the Ph.D. degree from Ghent University, Ghent, Belgium, in 1995 and 2000, respectively. From October 2000 to September 2002, he was with Lucent Technologies, Bell Laboratories, Murray Hill, NJ, USA, working on the design, processing, and characterization of InP/InGaAsP monolithically integrated devices. In October 2002, he joined the Department of Information Technology, INTEC, Ghent University, where he is currently a Full Professor. His research focuses on the design, fabrication, and characterization of integrated photonic devices.

Gunther Roelkens received the Degree in electrical engineering in 2002, and the Ph.D. degree in 2007, both from the Department of Information Technology, INTEC, Ghent University, Ghent, Belgium, where he is currently a Full Professor. In 2008, he was a Visiting Scientist with IBM TJ Watson Research Center, New York, NY, USA. His research interests include the heterogeneous integration of III-V semiconductors and other materials on top of silicon waveguide circuits and electronic/photonic cointegration. He was the holder of an ERC starting grant (MIRACLE) to start up research in the field of integrated mid-infrared photonic integrated circuits.